Interior versus boundary mixing of a cold intermediate layer

F. Cyr,[1] D. Bourgault,[1] and P. S. Galbraith[2]

Received 2 June 2011; revised 15 September 2011; accepted 6 October 2011; published 21 December 2011.

[1] The relative importance of interior versus boundary mixing is examined for the erosion of the cold intermediate layer (CIL) of the Gulf of St. Lawrence. Based on 18 years of historical temperature profiles, the seasonal erosion of the core temperature, thickness and heat content of the CIL are, respectively, $\dot{T}_{\min} = 0.24 \pm 0.04°C\ mo^{-1}$, $\dot{d}_{\min} = -11 \pm 2\ m\ mo^{-1}$ and $\dot{H} = 0.59 \pm 0.09\ MJ\ m^{-3}\ mo^{-1}$. These erosion rates are remarkably well reproduced with a one–dimensional vertical diffusion model fed with turbulent diffusivities inferred from 892 microstructure casts. This suggests that the CIL is principally eroded by vertical diffusion processes. The CIL erosion is best reproduced by mean turbulent kinetic energy dissipation rate and eddy diffusivity coefficient of $\epsilon \simeq 2 \times 10^{-8}\ W\ kg^{-1}$ and $K \simeq 4 \times 10^{-5}\ m^2\ s^{-1}$, respectively. It is also suggested that while boundary mixing may be significant it may not dominate CIL erosion. Interior mixing alone accounts for about 70% of this diffusivity with the remainder being attributed to boundary mixing. The latter result is in accordance with recent studies that suggest that boundary mixing is not the principal mixing agent in coastal seas.

Citation: Cyr, F., D. Bourgault, and P. S. Galbraith (2011), Interior versus boundary mixing of a cold intermediate layer, *J. Geophys. Res.*, *116*, C12029, doi:10.1029/2011JC007359.

1. Introduction

[2] Cold intermediate layers (CILs) are common summer feature of many subarctic coastal seas. Such water masses are found for example in the Black Sea [*Tuzhilkin*, 2008], the Baltic Sea [*Chubarenko and Demchenko*, 2010], the Bering Sea [*Kostianoy et al.*, 2004] the Sea of Okhotsk [*Rogashev et al.*, 2000], the Gulf of St. Lawrence [*Banks*, 1966] and can also be found in coastal oceans [*Petrie et al.*, 1988]. At formation, CILs may represent up to 45% of the total water volume of those systems [e.g., *Galbraith*, 2006] and therefore largely control the state and climate of subarctic coastal systems as well as the marine ecology [*Ottersen et al.*, 2004].

[3] The characteristics of CILs are principally governed by the properties of the surface mixed layer formed during the previous winter [*Gilbert and Pettigrew*, 1997; *Gregg and Yakushev*, 2005; *Galbraith*, 2006; *Smith et al.*, 2006a]. The CIL is formed when this surface mixed layer becomes insulated from the atmosphere by near-surface stratification caused by sea-ice melt, heat fluxes and increase runoff at the onset of spring. Other mechanisms such as horizontal/intra-layer convection may also contribute to CIL formation [*Chubarenko and Demchenko*, 2010].

[4] Most previous studies on CILs have focused on formation mechanisms but there is little published information about the summer deterioration of their properties by mixing processes, later recalled as *erosion*. One particularity of CILs is that since they lie at intermediate depths, away from surface and bottom boundary layers, one may hypothesize that their erosion is principally governed by interior mixing processes. However, CILs also intersect the sloping bottom around lateral boundaries where turbulent processes may be much more intense than within the interior. While the fraction of CIL volume in contact with the sloping bottom may be small the role of boundary mixing may still be important if turbulence is sufficiently large. This is analogous to the boundary mixing hypothesis proposed by *Munk* [1966] and *Munk and Wunsch* [1998] for the abyssal ocean but applied here to coastal seas. The idea of boundary mixing has been considered for mixing in sill fjords [*Stigebrandt*, 1976, 1979] and estuaries [*Bourgault and Kelley*, 2003; *Bourgault et al.*, 2008] with the hypothesis that breaking internal waves along sloping boundaries is the main mixing agent. It has also been proposed that boundary mixing may be the main contributor to the mixing budget of lakes [*Goudsmit et al.*, 1997], where wind-induced seiches are the principal driving mechanism, and to that of coastal seas with virtually no tides such as the Baltic Sea (see *Reissmann et al.* [2009] for a review). Other studies have however concluded that mixing in coastal seas is predominantly driven by interior rather than boundary processes [e.g., *MacKinnon and Gregg*, 2003; *Rippeth et al.*, 2005; *Palmer et al.*, 2008].

[5] Another interesting aspect of CILs is that they can be considered as passive tracers when the buoyancy-driven circulation of coastal seas is principally driven by salinity gradients. In this case, CILs are analogous to the yearly realization of a large-scale dye release experiment. Under this hypothesis, the CIL fills uniformly the entire sea and can only be modified, or eroded, by vertical turbulent processes.

[1]Institut des Sciences de la Mer de Rimouski, Université du Québec à Rimouski, Rimouski, Québec, Canada.
[2]Ocean and Environmental Science Branch, Maurice-Lamontagne Institute, Fisheries and Oceans Canada, Mont-Joli, Québec, Canada.

0148-0227/11/2011JC007359

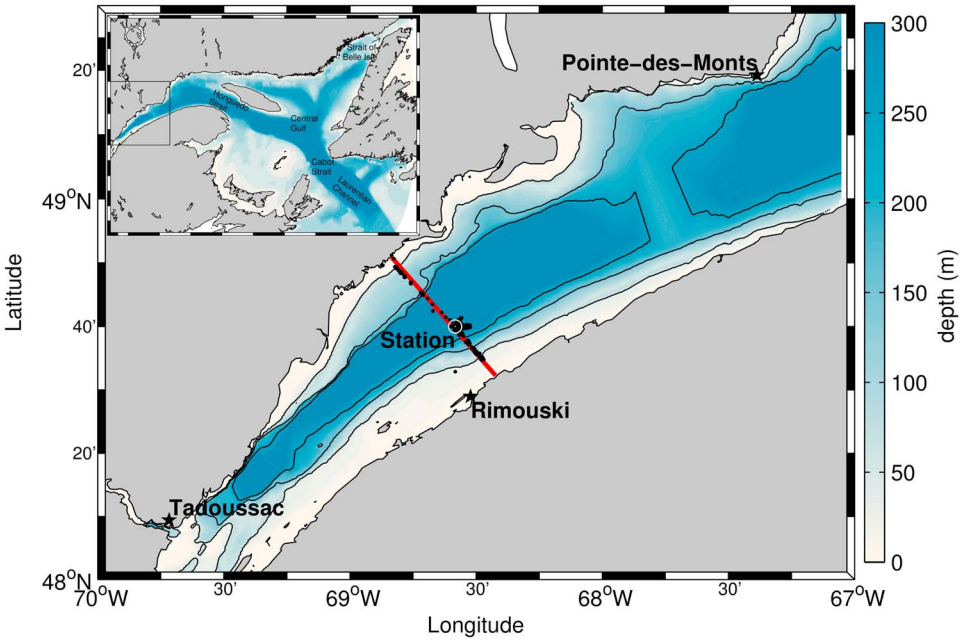

Figure 1. Location of 892 VMP casts (black dots) and bathymetric features of the St. Lawrence Estuary (figure) and the Gulf of St. Lawrence (inset). The black contour lines are the 50, 150 and 250 m isobaths. Rimouski station is identified with a white circle superimposed over the maximum profile concentration. The red line is the section referred to in Figure 12 and where sampling was performed during 10 days in July 2010.

[6] The objectives of this study are to examine whether vertical mixing alone can explain CIL erosion rates and, if so, to determine the relative importance of boundary versus interior mixing. To reach these objectives, we examine the erosion of the CIL in the Gulf of St. Lawrence using 18 years of historical CTD data, new turbulence measurements (892 casts) collected during summers 2009–2010 and a one-dimensional heat diffusion model. The historical CTD observations are used to provide statistics on CIL erosion rates and the turbulence measurements are used to provide eddy diffusivity values used in the one-dimensional model. After assessing the model we examine the relative importance of interior versus boundary mixing by comparing the modeled CIL erosion rates with and without considering diffusivity values measured near boundaries. The results are then interpreted based on a geometric scaling from which an effective eddy diffusivity is inferred and the relative contribution of boundary versus interior CIL mixing is determined.

2. The Gulf of St. Lawrence

[7] The Gulf of St. Lawrence, including the estuary, is an area of about 236000 km^2 opened to the Atlantic Ocean through Cabot Strait and the Strait of Belle Isle (Figure 1). The bathymetry is characterized by deep channels (>200 m), large shelves and islands. The main channel, called the Laurentian Channel, is a submarine glacial valley that runs from Tadoussac to the continental slope, past Cabot Strait (Figure 1). The residual circulation in this channel is estuarine-like, principally driven by the freshwater discharge of the St. Lawrence River and other surrounding rivers [e.g., *Koutitonsky and Bugden*, 1991]. In winter, the water column exhibits a two-layer structure with a 40–150 m thick surface mixed layer with temperature near the freezing point [*Galbraith*, 2006] overlying a warmer (1–6°C) but saltier (>33 psu) bottom layer of oceanic origin (roughly 150 m-bottom). The rest of the year, the water column is characterized with three layers with the CIL sandwiched between the warmer surface and bottom layers [*Koutitonsky and Bugden*, 1991].

[8] The CIL is characterized by near-freezing temperatures (T) and salinities (S) of 32–33 psu. Although the Gulf of St. Lawrence CIL is frequently mentioned in the literature, its definition varies between authors. For instance, *Lauzier and Bailey* [1957] used $T \leq 0$°C as their definition. Other authors have used other definitions such as $T \leq 1.5$°C [*Banks*, 1966; *Bugden et al.*, 1982], $T \leq 3$°C [*Gilbert and Pettigrew*, 1997; *Smith*, 2005] or more recently $T \leq 1$°C [*Galbraith et al.*, 2011]. Since the focus here is on the CIL erosion during ice-free months, we adopted the latter definition which approximately defines the coldest limit of what remains at the end of our study period, i.e., when the CIL is replenished the following winter.

[9] The CIL renewal occurs in winter when the surface mixed layer deepens following a combination of cold air temperature, wind–driven mixing and, to a lesser extent, brine rejection due to sea ice formation [*Galbraith*, 2006]. While the CIL is found throughout the Gulf, its presence at a given location may be due to horizontal advection from a remote formation site rather than resulting from local formation. For example, the region roughly located between Tadoussac and Pointe-des-Monts is too stratified, due to important freshwater input, to allow for winter convection and CIL formation [*Ingram*, 1979; *Galbraith*, 2006; *Smith et al.*, 2006b].

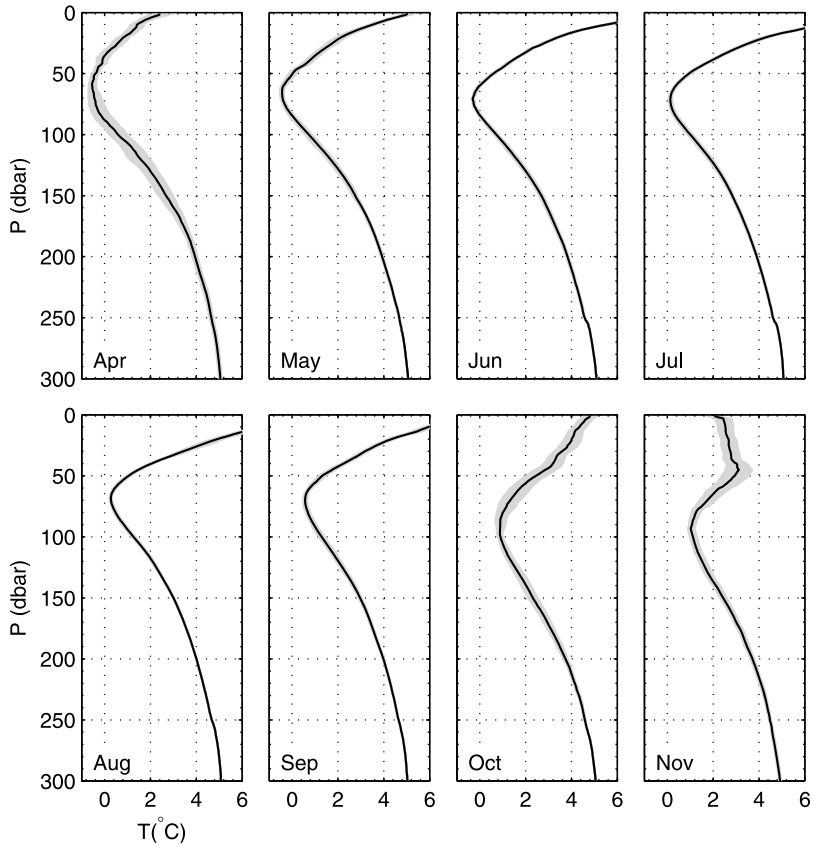

Figure 2. Monthly mean temperature profiles calculated from April to November over the period 1993–2010 from the CTD casts of Figure 4. The gray shadings are the 95% confidence intervals.

[10] While insights about CIL formation mechanisms were gained from previous field and modeling studies cited above, still little is known about CIL erosion mechanisms and rates. Based on 10 years of data from three regions of the Gulf (Honguedo Strait, Central Gulf and Cabot Strait), *Banks* [1966] found that from April to November the CIL minimum temperature (T_{min}) warms, on average, by 0.2°C mo^{-1}. Based on a similar analysis but using 47 years of data from five regions, *Gilbert and Pettigrew* [1997] obtained CIL erosion rates ranging from 0.08°C mo^{-1} for the Central Gulf to 0.30°C mo^{-1} for the Estuary. This study also revisits these warming rates.

3. Data Sets and Methodology

3.1. CTD Data

[11] The CTD dataset was collected at a station named *Rimouski* and located at 48°40′N 68°35′W, about 25 km north of the city of Rimouski (Figure 1). Thereafter, we will refer to this station as the interior station, i.e. a station in deep water (>300 m) away from lateral boundaries. This dataset consists of 418 casts collected by Maurice-Lamontagne Institute staff (Fisheries and Oceans Canada, DFO) between 1993 and 2010 and obtained through the DFO Oceanographic Data Management System [*Fisheries and Ocean Canada*, 2011]. The station is typically visited once a week during ice–free months [*Plourde et al.*, 2008] and, for the purpose of this study, only casts sampled between April and November have been selected. Temperature and salinity profiles were averaged into 1 m vertical bin size and all profiles of the same month have been averaged into a single monthly climatological profile (Figures 2 and 3). The 95% confidence intervals on the monthly averaged profiles have been estimated by performing 500 bootstrap replicates of each monthly sampling [*Efron and Gong*, 1983].

[12] Using this climatology, the depth-averaged volumetric heat content of the CIL was calculated as

$$H = \frac{1}{d}\int_{z_t}^{z_b} \rho c_p (T - T_f)\, dz \quad \text{for} \quad T < 1°\text{C}, \tag{1}$$

where d is the CIL thickness, z_t and z_b are, respectively, top and bottom limits of the layer, ρ is density determined from the equation of state of the seawater [*Fofonoff and Millard*, 1983] and c_p = 4.00 kJ kg^{-1}°C^{-1}, the specific heat of sea water, is considered constant. For convenience, the heat content is calculated relative to the typical freezing point temperature of sea water T_f = −1.8°C.

3.2. Sea Surface Temperature

[13] Since 2002, a meteorological buoy has been deployed at Rimouski station by the Maurice-Lamontagne Institute (DFO), usually from May to November when it then acquires data of various type every 15 minutes [*Fisheries and Ocean Canada*, 2011]. Among them, sea surface temperature (SST) is measured at 0.5 m below sea surface with a SBE-37SI, a temperature sensor manufactured by Sea-Bird Electronics.

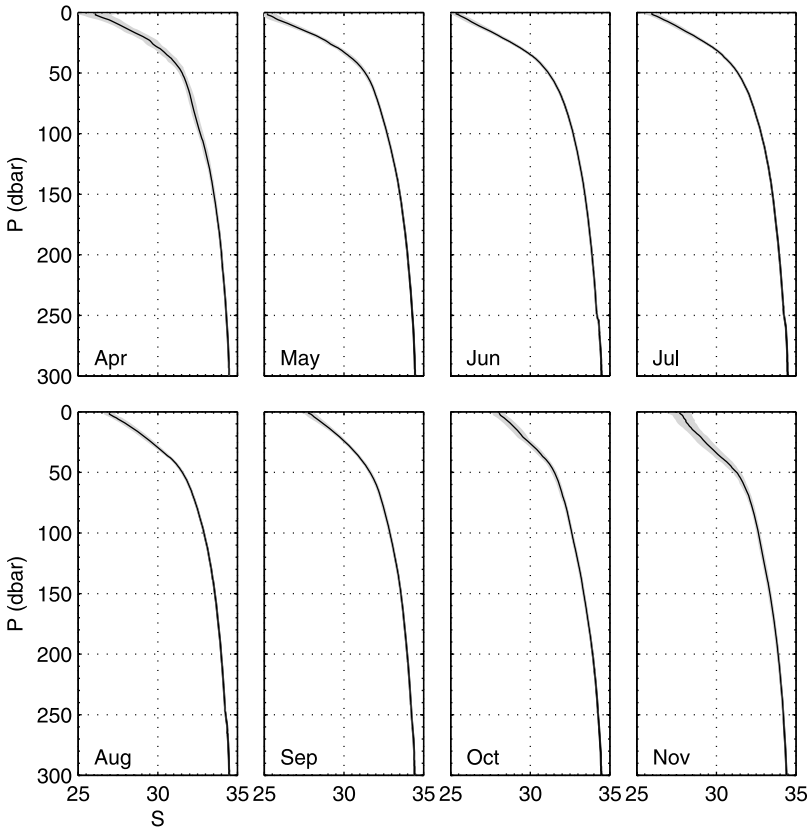

Figure 3. Monthly mean salinity profiles calculated as in Figure 2.

In this study, SSTs are used to provide boundary conditions to a one-dimensional model of heat diffusion presented in section 5.

3.3. Turbulence Measurements

[14] Turbulence measurements were collected with two free-fall, loosely-tethered, vertical microstructure profilers (VMP500) manufactured by Rockland Scientific International (RSI). Together with standard Sea-Bird Electronics CTD sensors, the VMPs are equipped with a micro-fluorescence/turbidity sensor, two fast-response thermistors and two airfoil shear probes which allow measurements of micro-scale vertical shear u'_z. One of the VMP also has a micro–conductivity sensor. All microstructure sensors sample at 512 Hz while the CTD samples at 64 Hz. See *Bourgault et al.* [2008] for more details on sensors and probes.

[15] Our dataset consists of 73 casts from 6 sorties done in July and September 2009 and 819 casts from 26 sorties done between May and October 2010. Most of these sorties were realized opportunistically, depending on weather and boat availability, except for a 10-days survey accomplished in July 2010. Two small craft boats, each carrying a VMP, were then mobilized to carry out sampling across the channel on a section passing through the Rimouski interior station. Overall, 420 casts out of 892 were realized within 5 km of Rimouski station (Figure 1). All together, these casts have no bias towards any phase of the M_2 tide cycle and are slightly biased toward neap tide (not shown). Uncertainties in mean quantities caused by this bias will be reflected in our analysis below through 95% confidence intervals obtained by bootstrapping. All surveys were carried out in relatively calm sea conditions. The wind speed was generally less than 20 km h^{-1} and wave heights less than 1 m.

[16] Assuming isotropic turbulence, the dissipation rate (ϵ) of turbulent kinetic energy was calculated, using standard procedures [e.g., *Lueck et al.*, 2002], as

$$\epsilon = \frac{15\nu}{2}\overline{(u'_z)^2}, \tag{2}$$

where $\nu = f(T)$ is the kinematic molecular viscosity as function of temperature and the overline indicates here a 5-m scale spatial average. The shear variance $(u'_z)^2$ was obtained by spectral integration to remove random noise. Eddy diffusivity coefficients were calculated as [*Osborn*, 1980]

$$K = \Gamma\frac{\epsilon}{N^2}, \tag{3}$$

where Γ is the dissipation flux coefficient and N is the 5-m scale background buoyancy frequency. Using $\Gamma = 0.2$ [*Osborn*, 1980; *Moum*, 1996], an upper bound for the eddy diffusivity coefficient was determined. An estimation of the 95% confidence intervals of the mean turbulence profile was obtained by performing 500 bootstrap replicates of the sampling set.

4. Observations

4.1. CIL Characteristics and Variability

[17] The CIL structure and variability for the 1993–2010 period can be qualitatively appreciated in Figure 4. During

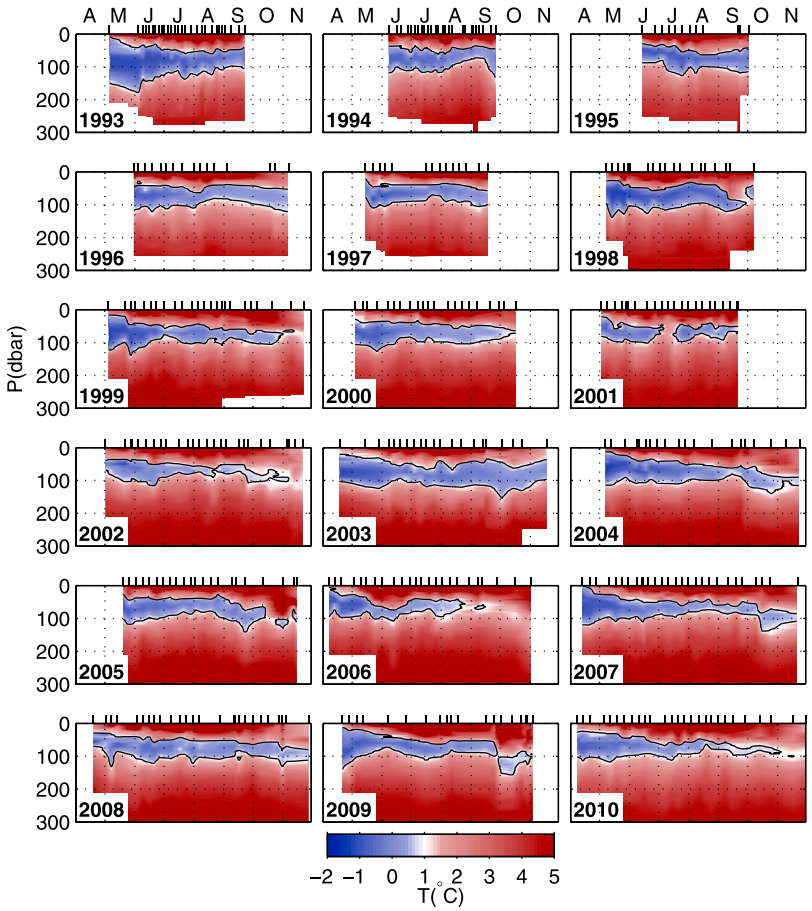

Figure 4. Evolution of temperature profiles from April to November, linearly interpolated from 418 CTD casts that are indicated by lines at the top of each figure. To focus on the CIL, the color scale is saturated at 5°C while summer surface temperature can reach more than 10°C, and 1°C isotherms are highlighted with a black contour.

spring, the CIL is roughly 50–100 m thick and centered around 60 m. It persists throughout summer and fall until it becomes regenerated and replenished the following winter. The temperature field within the CIL exhibits important intraseasonal variability. For example, in 2001 isotherms displacement reached 50 m and the minimum CIL temperature varied by ~1°C on monthly timescales. The CIL even disappeared, according to our definition, for a 2-week period at the beginning of July. A striking feature often occurs in fall (e.g., 2004, 2007 and 2009), when within about a week, the CIL suddenly plunges downward by approximately 50 m. The origin of these intraseasonal variations is unknown and will not be addressed in this study.

[18] The evolution of monthly averaged profiles reveal that the temperature (Figure 2) and the salinity (Figure 3) of the surface layer increases from April to August. While the salinity of this layer continues to increase from September to November, the layer rapidly cools and deepens during the same period. Underneath the surface layer, that is under 50 m, the CIL temperature minimum increases from April to November while the salinity stays relatively constant. We interpret this as an indication that the mid-depth salinity field is approximately in steady state ($\frac{\partial S}{\partial t} \simeq 0$) during ice-free months, likely due to a balance between longitudinal advection and vertical diffusion. Unlike the salinity, no equivalent compensating source of cold water that can feed the CIL once it has been replenished during winter. The CIL thus acts like a passive tracer, being slowly mixed by vertical diffusion.

[19] The monthly climatology of the temperature distribution within the CIL (Figure 2) can be synthesized in a single contourplot that reveals the general characteristics of the CIL and its seasonal erosion (Figure 5a). From April to November the CIL thickness steadily decreases while the minimum temperature increases. This erosion can be quantified by examining the evolution of the climatological minimum temperature of the CIL $T_{\min}$ (Figure 6a), which increases linearly at a rate of $\dot{T}_{\min} = 0.24 \pm 0.04°C\ mo^{-1}$, as determined by performing linear best fits to the climatological timeseries. The error reported is the standard error determined by bootstrap analysis [*Efron and Gong*, 1983]. The erosion of the CIL can also be quantified by the rate of its thickness decrease which is $\dot{d} = -11 \pm 2\ m\ mo^{-1}$ (Figure 6b). Finally, the seasonal change in CIL mean heat content is $\dot{H} = 0.59 \pm 0.09\ MJ\ m^{-3}\ mo^{-1}$ (Figure 6c). Note that the sudden fall deepening events of the CIL observed in Figure 4 clearly

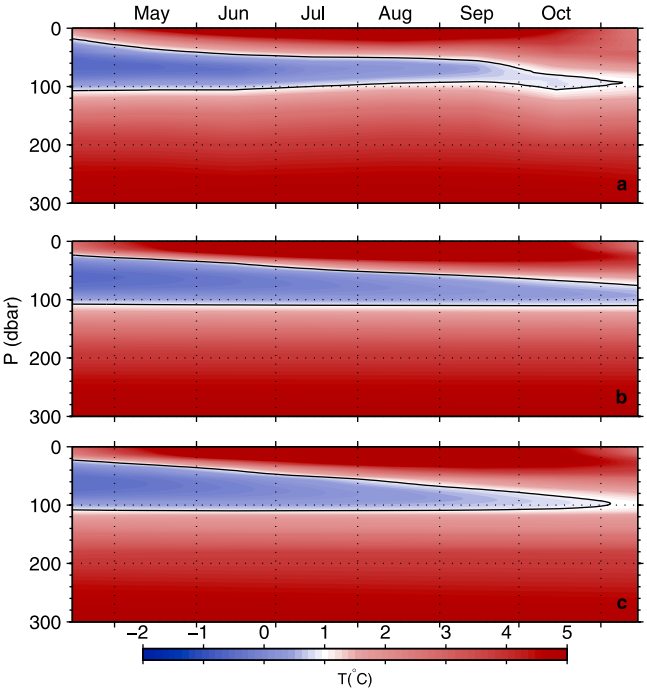

Figure 5. April to November water temperature. (a) Monthly climatology over the period 1993–2010 calculated from the CTD casts of Figure 4. (b) Modeled evolution of temperature using the observed mean interior diffusivity profile K_i. (c) Modeled evolution of temperature using the diffusivity profile from all available casts K_a. Figure properties are the same as Figure 4.

show up in the monthly temperature climatology (Figure 5a) and also in the climatological evolution of CIL core depth (Figure 6d). The CIL also shows interannual variability of the warming rate of the CIL core (Figure 7), reaching values as high as $\dot{T}_{\min} = 0.30°C\ mo^{-1}$ (1999 and 2004) and as low as $\dot{T}_{\min} = 0.15°C\ mo^{-1}$ (1997 and 2003). Note that years 2009 and 2010, i.e., the years that turbulence was sampled were climatologically close-to-normal (Figure 7).

4.2. Turbulence

[20] A typical VMP cast is shown in Figure 8 providing profiles of temperature T, density ρ, microstructure shear u'_z, turbulent dissipation rate ϵ and eddy diffusivity K. Turbulence within the CIL (gray intervals in Figure 8) is typically low compared to patches of much higher dissipation often found in the top 50 m or so of the water column.

[21] Turbulence measurements collected in 2009 and 2010 are synthesized in Figure 9. Two series of mean profiles are presented, i.e., the average of all available casts (892), including interior and boundary regions (dark gray, solid line), and the average of interior casts only (light gray, dashed-line). Globally, highest dissipation rates and diffusivities are found in the top 20 m or so of the water column with values reaching $\epsilon \sim 10^{-6}$ W kg^{-1} and $K \sim 10^{-3}$ m^2 s^{-1}. Under 20 m, there is a decreasing trend of the dissipation and the diffusivity with depth; the increase in dissipation and diffusivity observed near 130 m likely comes from the numerous turbulence casts made on the shelf that passed through the bottom boundary layer at that depth. When considering only interior casts (420), the mean dissipation rate and diffusivity underneath the surface layer (20–180 m) are, respectively, $\overline{\epsilon}_i = 1.3(0.9, 1.7) \times 10^{-8}$ W kg^{-1} and $\overline{K}_i = 2.4(1.5, 3.5) \times 10^{-5}$ m^2 s^{-1}, where the numbers in parentheses are the bootstrap 95% confidence intervals. When considering all available casts (892), the mean dissipation and diffusivity for the same depth range are respectively $\overline{\epsilon}_a = 1.9(1.3, 2.8) \times 10^{-8}$ W kg^{-1} and $\overline{K}_a = 4.3(2.6, 6.6) \times 10^{-5}$ m^2 s^{-1}, i.e., respectively 1.5 and 1.8 times higher than when considering only interior casts.

[22] These diffusivities are close to an order of magnitude smaller than that previously inferred by *Bugden* [1991] from least square fit on temperature data in the Gulf between 200–300 m and on the same order than that inferred by *Ingram* [1979] near Tadoussac in the 50–100 m depth range.

5. Heat Diffusion Model

5.1. Model Description

[23] We now examine with a one-dimensional heat diffusion model whether the turbulence measured during calm conditions could explain the observed climatological CIL erosion rates. With this approach we neglect horizontal

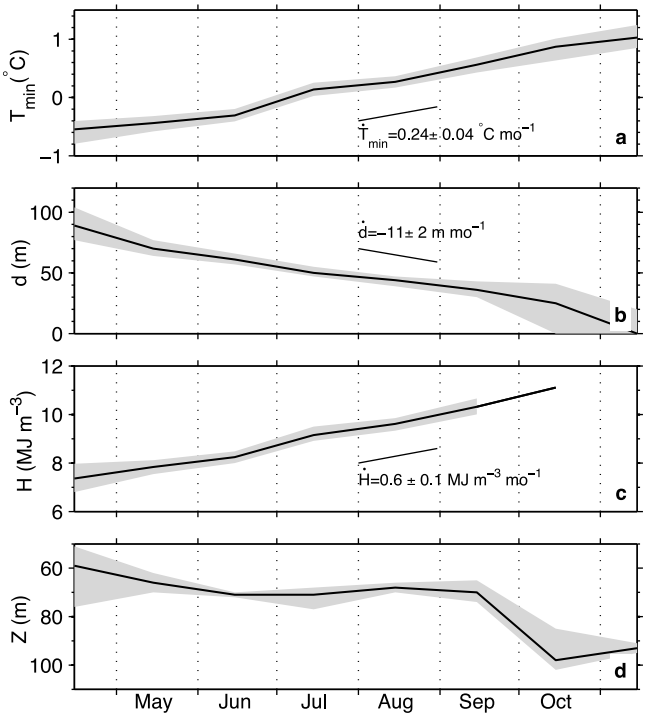

Figure 6. Evolution of CIL properties. Solid lines are monthly averages over the period 1993–2010. The shaded areas are the 95% confidence interval. (a) Temperature of the CIL core, (b) thickness of the CIL, (c) heat content of the CIL and (d) depth of the CIL core. Thin short lines in Figures 6a–6c are the mean slopes (erosion rates) calculated in section 4.1. The mean slope is reported on figures with the 95% confidence intervals (see Table 1 for comparison with model results).

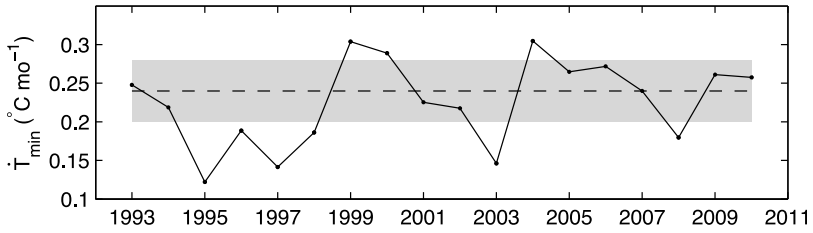

Figure 7. Interannual variability of the warming rate of the CIL core, calculated between April and November for every year over the period 1993–2010. The warming rate is defined as the slope of the best linear fit of the evolution of the CIL core temperature as shown in Figure 6a. The dashed line is the average warming rate (0.24°C mo^{-1}) and the shaded area is the 95% confidence interval envelope (±0.04°C mo^{-1}).

advection under the assumption that only vertical turbulent mixing can redistribute heat within the water column.

[24] The model numerically solves the following equation for the temporal evolution of the water column temperature $T(z, t)$ [e.g., *Kundu and Cohen*, 2007]:

$$\frac{\partial T}{\partial t} = \frac{\partial}{\partial z}\left(K\frac{\partial T}{\partial z}\right), \tag{4}$$

where K is the eddy diffusivity of heat taken here to be equivalent to the eddy diffusivity of mass as defined in equation (3) [*Thorpe*, 2007]. Eddy diffusivity is assumed to be variable with depth but constant in time, i.e, $K = K(z)$.

[25] Equation (4) is solved numerically with a first-order Euler scheme on a grid size $\Delta z = 1$ m and using a time step $\Delta t = 100$ s. The vertical resolution thus adequately resolve the different layers and fits the resolution of CTD bins. The time step respects the Courant-Friedrich-Levy stability condition. A no-flux boundary condition is applied at the sea bottom fixed at $z = 300$ m. A daily climatological sea surface temperature (SST) is imposed as boundary conditions at the top of the water column. This climatology was evaluated over the period 2002–2009 using observations from the oceanographic buoys [*Fisheries and Ocean Canada*, 2011] and interpolated to the model time step Δt. Equation (4) was initialized with the climatological temperature profile for April (Figure 2).

[26] Two simulations were carried out with different heat diffusivity profiles. The first simulation uses the mean interior diffusivity profile K_i, while the second uses the mean diffusivity profile of all casts collected across the channel, i.e., K_a (Figure 9). Since no casts were done deeper then about 180 m, K_i and K_a are extended to 300 m using a constant value equal to the minimum value of the mean profile.

[27] Note that this model is designed to examine the average seasonal evolution of the temperature structure and

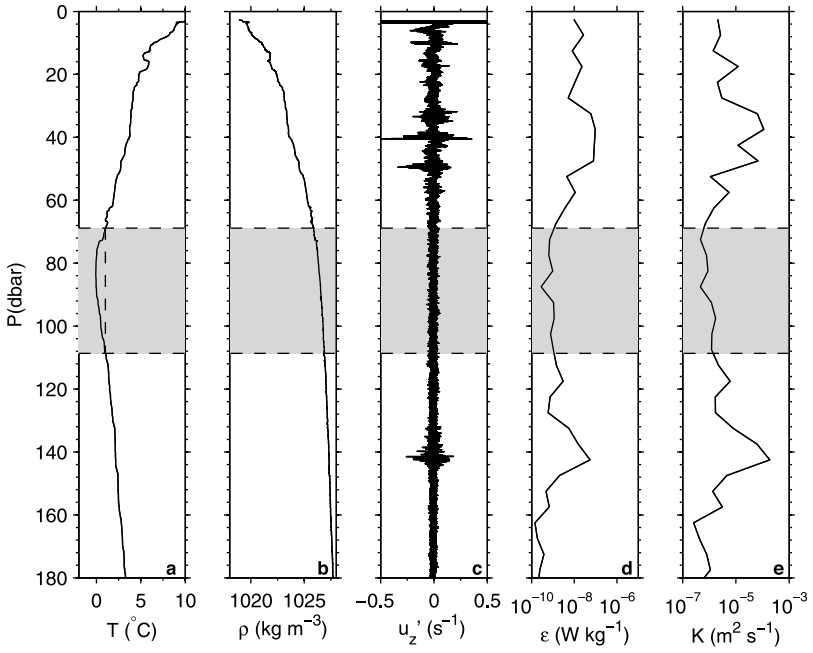

Figure 8. Typical turbulence profiler measurements, from July 21 2009. (a–c) Unfiltered profiles (temperature, sea water density and vertical shear), i.e., sampled at 64 Hz for T and ρ and 512 Hz for u'_z. (d and e) Five-m scale TKE dissipation rate, ϵ, and eddy diffusivity, K. The CIL has been highlighted in Figure 8a and its depth is reported on all figures as shaded areas.

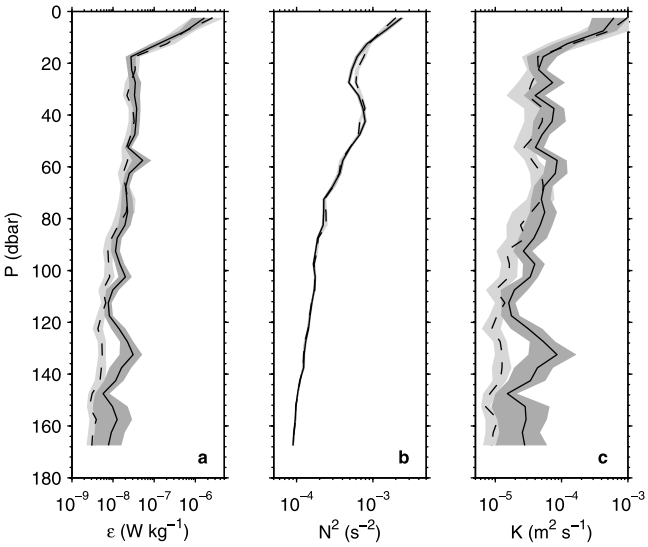

Figure 9. Mean quantities from all 892 VMP casts for 2009–2010 (dark gray, solid lines). (a) Mean dissipation rate of turbulent kinetic energy, (b) mean buoyancy frequency squared and (c) mean eddy diffusivity coefficient. The gray shades indicate 95% confidence intervals. Mean quantities for casts taken at mid-channel (420) are also presented (light-gray, dashed-lines).

not a particular year. For this reason, the model is forced with quasi climatological boundary conditions. For consistency, a climatological profile of eddy diffusivity should also be used. However, such statistics are not available. We therefore work under the assumption that the turbulence measured in 2009 and 2010 are representative of long-term mean conditions. This appears to be a reasonable assumption given that years 2009–2010 were subject to close-to-normal erosion rates (Figure 7).

5.2. Results

[28] While the model has difficulties to reproduce the evolution of the surface layer above 50 m (see *Doyon and Ingram* [2000] for a similar model of the surface mixed layer) it reproduces qualitatively well the CIL from April to November (Figures 5 and 10). Overall, the simulation using K_a better reproduces the observations except perhaps for the month of June where using K_i offers a slight improvement (Figure 10). The better performance of the model with K_a instead of K_i is also seen when examining a space–time contour plot of $T(z, t)$ (Figure 5).

[29] Quantitatively, the simulation with K_a reproduces remarkably well, i.e., within the uncertainties, the CIL erosion rates (Figure 11 and Table 1). In this case, the modeled and observed erosion rates (i.e., $\dot{T}_{\min}$, $\dot{d}$ and $\dot{H}$) agree to within 8% or better. On the other hand, using only the

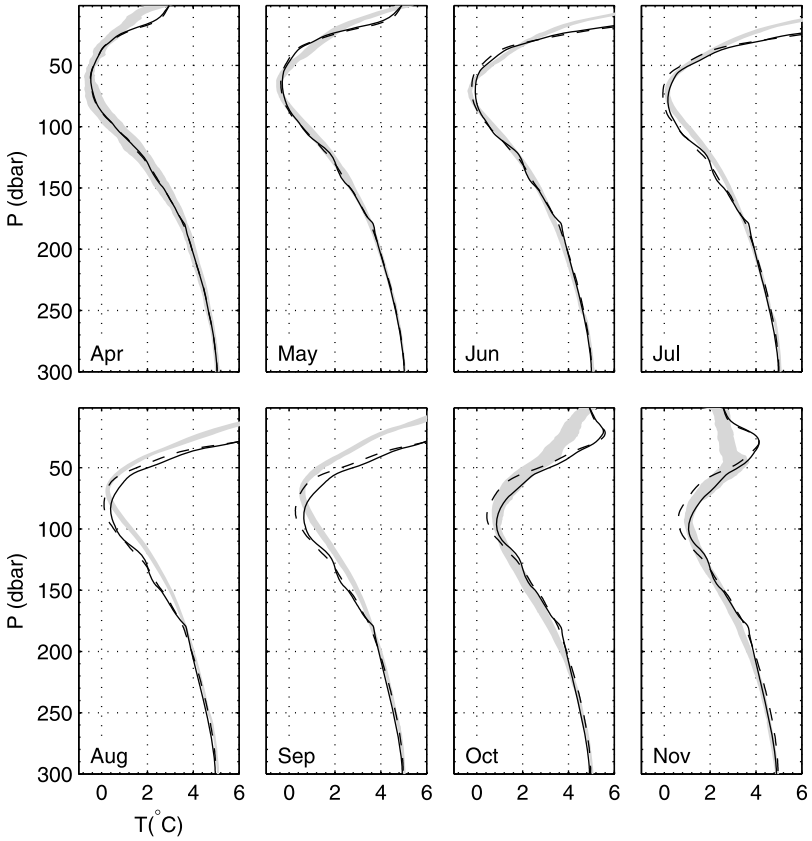

Figure 10. Details of the evolution of monthly mean temperature profiles for observations and simulations. The observed 95% confidence intervals of the observed mean temperature profile (shaded area) is compared to two simulations done with respectively the average observed diffusivity at mid-channel K_i (dashed lines) and from all available casts along the section K_a (solid lines).

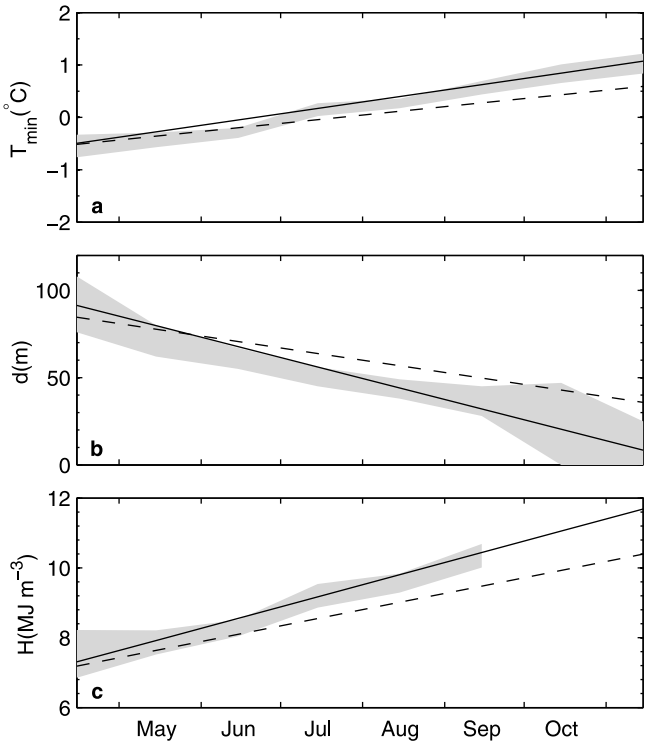

Figure 11. Comparison between observed and modeled CIL erosion rates: (a) core temperature, (b) thickness and (c) heat content. 95% confidence interval of the observations (1993–2010) are presented, together with the linear best fits of the monthly means from the model when forced respectively with K_i (dashed lines) and K_a (solid lines). All slopes are provided in Table 1.

interior diffusivity K_i accounts for about 65% of the observed erosion rates.

6. Discussion

[30] Our analysis suggests that interior diffusivity during calm wind conditions (Figure 9) accounts for about 65% of the mid-channel CIL erosion rate (Table 1). However, the apparent missing mixing is recovered when all profiles collected throughout the section are included in the analysis. This suggests that non-local boundary mixing processes, although not dominant, may contribute significantly to mid-channel erosion.

Table 1. Slopes of Linear Best Fits for Figure 11[a]

	$\dot{T}_{\min}$ (°C mo^{-1})	$\dot{d}$ (m mo^{-1})	$\dot{H}$ (MJ m^{-3} mo^{-1})
Climatology of observations	0.24	−11	0.59
Model, K_i	0.16	−7	0.46
Model, K_a	0.22	−12	0.63

[a]The three columns are respectively the CIL core temperature warming rate, the CIL thinning rate and the rate of increase in CIL heat content. Each is calculated for the climatology of CTD observations (1993–2010), the modeled temperature diffusion using respectively the interior diffusivity profile K_i and the the mean diffusivity profile from all available casts K_a.

[31] With this in mind, we now examine the role that boundary mixing may play in eroding the CIL at mid-channel. We start by assuming that, on monthly time-scales, there is a continuous exchange of properties along isopycnals between boundaries, where the CIL intersects the sloping bottom and the interior. Inspired by *Armi* [1978], *Garrett and Gilbert* [1988], *Garrett et al.* [1993] and *Toole et al.* [1997], we estimate the effective diffusivity coefficient using the following geometric scaling:

$$K_e = K_b \frac{A_b(z,h_b)}{A(z)} + \tilde{K}_i \frac{A_i(z,h_b)}{A(z)}, \tag{5}$$

where K_e is the effective diffusivity coefficient at depth z, while K_b and $\tilde{K}_i$ are, respectively, constant diffusivity coefficients within the bottom boundary layer and in the interior, and h_b the bottom boundary layer thickness. Similarly, $\frac{A_b}{A}$ and $\frac{A_i}{A} = 1 - \frac{A_b}{A}$ are respectively the fraction of the CIL inside and outside the bottom boundary layer of thickness h_b at depth z (Figure 12). Note that unlike the previously cited authors, we kept in the formulation for K_e the contribution from interior mixing (i.e., the second term in equation (5)), since we have indications that boundary mixing is not dominant in front of interior mixing.

[32] The thickness of the bottom boundary layer h_b was visually-inferred by inspecting the vertical structure of the dissipation rates ϵ of 150 casts, out of 892, that hit the bottom out of the 892 (Figure 13). On average, these measurements show an approximate exponential growth of ϵ towards the bottom, starting at about 10 m above the bottom. Based on these measurements we set $h_b = 1 \times 10^1$ m.

[33] Considering the climatological CIL limits from our observations (Figure 5a) and assuming that the depth spanned by the CIL is uniform across the section, the fraction of the CIL area within the bottom boundary layer varies between 2–3% between April and October (the CIL

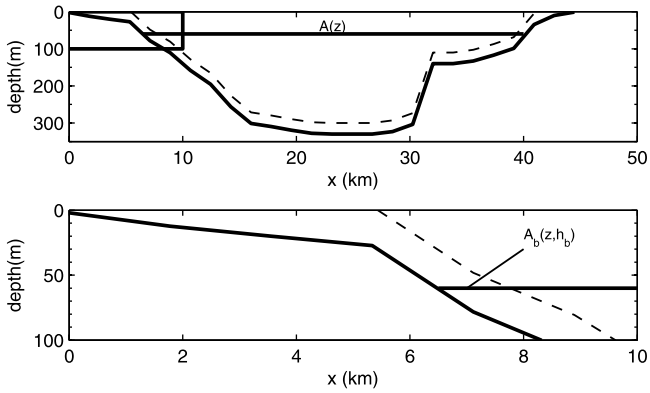

Figure 12. Details of the geometric scaling used to calculate the "apparent" eddy diffusivity (equation (5)). (top) Bathymetric section of the estuary at Rimouski station (see Figure 1, red line). (bottom) Enlargement of the rectangle in Figure 12 (top). For both figures, x is the distance from the South shore. The dashed line corresponds to the upper limit of the bottom boundary layer of height h_b (not to scale for emphasis). $A(z)$ is the channel width at depth z and $A_b(z, h_b)$ is the width of $A(z)$ within the boundary layer.

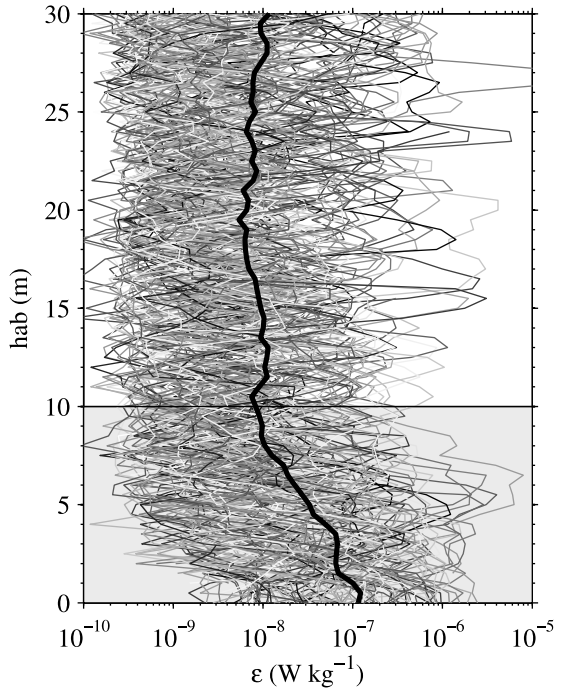

Figure 13. All dissipation rate profiles (150) that hit the bottom (gray curves) and their mean (thick black curve). Data are presented relative to height above bottom (hab). The gray shaded area highlights the visually-inferred 10-m thick bottom boundary layer.

has disappeared by November according to our climatology). In other words,

$$\overline{\left(\frac{A_b(z,h_b)}{A(z)}\right)} = \overline{\frac{1}{(z_t - z_b)}\int_{z_t}^{z_b} \frac{A_b(z,10\text{ m})}{A(z)}\,\mathrm{d}z} \simeq 3\%, \qquad (6)$$

where z_t and z_b are the climatological CIL limits and the overline indicates an average in time between April and October.

[34] We extracted from our measurements the mean diffusivity that is within the bottom boundary layer (h_b = 1 × 10^1 m) using casts that reached the bottom. This yielded K_b = 3.3(2.1, 4.8) × 10^{-4} m^2 s^{-1}. Letting $\tilde{K}_i = \overline{K}_i$ = 2.4(1.5, 3.5) × 10^{-5} m^2 s^{-1}, i.e. the measured interior diffusivity (Section 4.2), equation (5) gives K_e = 3.3 × 10^{-5} m^2 s^{-1}. This value is slightly lower, but within confidence intervals, than $\overline{K}_a$, i.e., the depth-averaged diffusivity of all profiles collected across the section (Section 4.2). We note also that both terms in equation (5) are significant in the mixing budget, but their contribution to the effective diffusivity is not the same. Our scaling suggests that the interior mixing supplies 70% of the effective diffusivity while the boundary mixing supplies the remaining 30%. We conclude from this analysis that boundary mixing may contribute to the CIL erosion observed at mid-channel but that its role is not dominant in front of interior mixing.

[35] To examine whether this analysis is relevant to a broader geographical context, we calculated the fraction of the volume of the CIL found within the bottom boundary layer throughout the Gulf of St. Lawrence. This calculation was done using historical CIL data for the months of August and September between 1995 and 2010 (see *Galbraith et al.* [2011] and *Tamdrari et al.* [2011] for details) and assuming a 10-m thick bottom boundary layer throughout the Gulf. The result suggests that, on average, 6 ± 1% of the Gulf's CIL is within the bottom boundary layer. This fraction is about twice as large as the value inferred from our sampling section. This suggests that boundary mixing may be more important throughout the Gulf than at our sampling section off Rimouski. This possibility is highlighted when examining the area throughout the Gulf where the CIL intersects the sloping bottom (Figure 14). On average during this

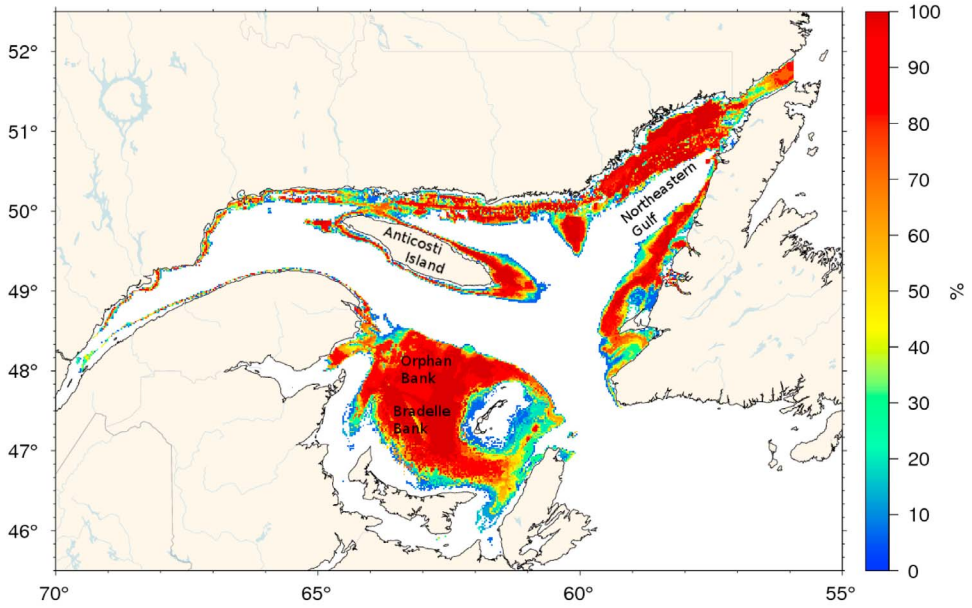

Figure 14. Occurrence of the CIL that reaches the seabed (1995 to 2010). The white regions are where the CIL never reached the seabed.

period, the CIL is in contact with approximately 30% of the Gulf's seabed. Regions where the CIL reached the seabed more often are located in the Southern Gulf (Bradelle and Orphan Banks), Northeastern Gulf and the bank off of the western tip of Anticosti Island. These regions may therefore contribute substantially to CIL erosion.

7. Conclusion

[36] Two goals were pursued in this study: 1) to test a model of vertical diffusion for the erosion of a CIL and; 2) to discuss the importance of boundary versus interior mixing on this erosion. The seasonal erosion of the core temperature, thickness and heat content of the Gulf of St. Lawrence CIL off Rimouski are, respectively, $\dot{T}_{\min} = 0.24 \pm 0.04°C\ mo^{-1}$, $\dot{d}_{\min} = -11 \pm 2\ m\ mo^{-1}$ and $\dot{H} = 0.59 \pm 0.09\ MJ\ m^{-3}\ mo^{-1}$. These rates are remarkably well reproduced with a one-dimensional diffusion model fed with observed turbulent diffusivities. This suggests that the CIL is principally eroded by vertical diffusion processes. Our analysis further suggests that interior mixing processes contribute to approximately 70% to this erosion with the remaining being attributed to boundary mixing. This conclusion supports recent studies [e.g., *MacKinnon and Gregg*, 2003; *Rippeth et al.*, 2005; *Palmer et al.*, 2008] that also proposed that boundary mixing may not be the predominant mixing source in coastal seas. However, it would be relevant to extend this study to other regions of the Gulf where boundary mixing may be more important.

[37] It is unclear at this point what mixing mechanisms operate either in the interior or at boundaries. Given that our analysis is based on observations collected during calm wind conditions leads us to believe that wind plays a secondary role in eroding the CIL. Internal shear associated with the internal tide that can cause up to 20 m isopycnal displacement is the most likely candidate for producing turbulence in the interior. Near sloping boundaries where the CIL intersects the bottom, internal wave breaking and bottom shear stresses are likely at work. It is not possible to conclude at this point on the modulation of the mixing with the M_2 and neap/spring tide cycles. Preliminary results (not presented) however suggest that while the neap/spring cycle has no incidence on the interior mean diffusivity, it can modulate the mean diffusivity at boundaries by up to a factor of two. However, new field experiments are required to make further progress in those directions.

[38] **Acknowledgments.** This work was funded by Le Fonds de recherche du Québec – Nature et technologies, the Natural Sciences and Engineering Research Council of Canada, the Canada Foundation for Innovation and Fisheries and Oceans Canada and is a contribution to the scientific program of Québec-Océan. The authors would also like to thank Pierre Joly and his collaborators for their sampling effort since 1993, now part of the Atlantic Zonal Monitoring Program, as well as the technicians and students who helped in our 2009 and 2010 summer campaigns: Bruno Cayouette, Rémi Desmarais, Gilles Desmeules, Sylvain Leblanc, Camil Hamel, Joachim Bobinet and Guillaume Turbide. Thanks also to Richard Dewey for sharing his code for calculating dissipation rates and to Barry Ruddick for his helpful comments.

References

Armi, L. (1978), Some evidence of boundary mixing in the deep ocean, *J. Geophys. Res.*, *83*(C4), 1971–1979.

Banks, R. E. (1966), The cold layer in the Gulf of St. Lawrence, *J. Geophys. Res.*, *71*(6), 1603–1610.

Bourgault, D., and D. E. Kelley (2003), Wave-induced boundary mixing in a partially mixed estuary, *J. Mar. Res.*, *61*, 553–576.

Bourgault, D., D. E. Kelley, and P. S. Galbraith (2008), Turbulence and boluses on an internal beach, *J. Mar. Res.*, *66*(5), 563–588.

Bugden, G. L. (1991), Changes in the temperature-salinity characteristics of the deeper waters of the Gulf of St. Lawrence, *Can. Spec. Publ. Fish. Aquat. Sci.*, *113*, 139–147.

Bugden, G. L., B. T. Hargrave, M. M. Sinclair, C. L. Tang, J.-C. Theriault, and P. A. Yeats (1982), Changes in the temperature-salinity characteristics of the deeper waters of the Gulf of St. Lawrence over the past several decades, *Can. Spec. Publ. Fish. Aquat. Sci.*, *1078*, 1–89.

Chubarenko, I., and N. Demchenko (2010), On contribution of the horizontal and intra-layer convection to the formation of the Baltic Sea cold intermediate layer, *Ocean Sci.*, *6*, 285–299.

Doyon, P., and R. G. Ingram (2000), Seasonal upper-layer T-S structure in the Gulf of St. Lawrence during ice-free months, *Deep Sea Res. Part II*, *47*, 385–413.

Efron, B., and G. Gong (1983), A leisurely look at the bootstrap, the jackknife and cross-validation, *Am. Stat.*, *37*(1), 36–48.

Fisheries and Ocean Canada (2011), ODMS—Oceanographic Data Management System, http://ogsl.ca/app-sgdo/en/accueil.html, Mont-Joli, Que., Canada.

Fofonoff, P., and R. J. Millard (1983), Algorithms for computation of fundamental properties of seawater, *UNESCO Tech. Pap. Mar. Sci. 44*, U. N. Educ., Sci. and Cult. Organ., Paris.

Galbraith, P. S. (2006), Winter water masses in the Gulf of St. Lawrence, *J. Geophys. Res.*, *111*, C06022, doi:10.1029/2005JC003159.

Galbraith, P. S., R. G. Pettipas, J. Chassé, D. Gilbert, P. Larouche, B. Pettigrew, A. Gosselin, L. Devine, and C. Lafleur (2011), Physical oceanographic conditions in the Gulf of St. Lawrence in 2010, *Can. Sci. Advis. Secr. Res. Doc. 2011/045*, iv + 83 pp., Fish. and Oceans Can., Québec, Que., Canada.

Garrett, C., and D. Gilbert (1988), Estimates of vertical mixing by internal waves reflected off a sloping bottom, in *Small-Scale Turbulence and Mixing in the Ocean: Proceedings of the 19th International Liege Colloquium on Ocean Hydrodynamics*, edited by J. C. J. Nihoul and B. M. Jamart, pp. 405–424, Elsevier, New York.

Garrett, C., P. MacCready, and P. Rhines (1993), Boundary mixing and arrested Ekman layers: Rotating stratified flow near a sloping boundary, *Annu. Rev. Fluid Mech.*, *25*, 291–323.

Gilbert, D., and B. Pettigrew (1997), Interannual variability (1948–1994) of the CIL core temperature in the Gulf of St. Lawrence, *Can. J. Fish. Aquat. Sci.*, *54*, 57–67.

Goudsmit, G., F. Peeters, M. Gloor, and A. Wüest (1997), Boundary versus internal diapycnal mixing in stratified natural waters, *J. Geophys. Res.*, *102*, 27,903–27,914.

Gregg, M. C., and E. Yakushev (2005), Surface ventilation of the Black Sea's cold intermediate layer in the middle of the western gyre, *Geophys. Res. Lett.*, *32*, L03604, doi:10.1029/2004GL021580.

Ingram, R. G. (1979), Water mass modification in the St. Lawrence estuary, *Nat. Can.*, *106*, 45–54.

Kostianoy, A. G., J. C. J. Nihoul, and V. B. Rodionov (2004), *Physical Oceanography of Frontal Zones in the Subarctic Seas*, *Elsevier Oceanogr. Ser.*, vol. 71, 316 pp., Elsevier, Amsterdam.

Koutitonsky, V. G., and G. L. Bugden (1991), The physical oceanography of the Gulf of St. Lawrence: A review with emphasis on the synoptic variability of the motion, *Can. Spec. Publ. Fish. Aquat. Sci.*, *113*, 57–90.

Kundu, P. K., and I. M. Cohen (2007), *Fluid Mechanics*, 4th ed., 872 pp., Academic, Burlington, Mass.

Lauzier, L. M., and W. B. Bailey (1957), Features of the deeper waters of the Gulf of St. Lawrence, *Bull. Fish. Res. Board Can.*, *111*, 213–250.

Lueck, R. G., F. Wolk, and H. Yamasaki (2002), Oceanic velocity microstructure measurements in the 20th century, *J. Oceanogr.*, *58*, 153–174.

MacKinnon, J. A., and M. C. Gregg (2003), Mixing on the late-summer New England shelf-solibores, shear and stratification, *J. Phys. Oceanogr.*, *33*, 1476–1492.

Moum, J. N. (1996), Efficiency of mixing in the main thermocline, *J. Geophys. Res.*, *101*(C5), 12,057–12,069.

Munk, W. H. (1966), Abyssal recipes, *Deep Sea Res.*, *13*, 707–730.

Munk, W. H., and C. Wunsch (1998), Abyssal recipes II: energetics of tidal and wind mixing, *Deep Sea Res. Part I*, *45*, 1977–2010.

Osborn, T. R. (1980), Estimates of the local rate of vertical diffusion from dissipation measurements, *J. Phys. Oceanogr.*, *10*, 83–89.

Ottersen, G., J. Alheit, K. Drinkwater, K. Friedland, E. Hagen, and N. C. Stenseth (2004), The responses of fish populations to ocean climate fluctuations, in *Marine Ecosystems and Climate Variations*, edited by N. C.

Stenseth, G. Ottersen, J. W. Hurrel, and A. Belgrano, chap. 6, pp. 73–94, Oxford Univ. Press, Oxford, U. K.

Palmer, M. R., T. P. Rippeth, and J. H. Simpson (2008), An investigation of internal mixing in a seasonally stratified shel sea, *J. Geophys. Res.*, *113*, C12005, doi:10.1029/2007JC004531.

Petrie, B., S. A. Akenhead, S. A. Lazier, and J. Loder (1988), The cold intermediate layer on the Labrador and northeast Newfoundland shelves, 1978–86, *Northwest Atl. Fish. Organ. Sci. Counc. Stud.*, *12*, 57–69.

Plourde, S., P. Joly, L. St-Amand, and M. Starr (2008), La station de monitorage de Rimouski: Plus de 400 visites et 18 ans de monitorage et de recherche, *Atl. Zone Monit. Program Bull.*, *8*, 51–55.

Reissmann, J. H., H. Burchard, R. Feistel, E. Hagen, H. U. Lass, V. Mohrholz, G. Nausch, L. Umlauf, and G. Wieczorek (2009), Vertical mixing in the Baltic Sea and consequences for eutrophication—A review, *Prog. Oceanogr.*, *82*(1), 47–80, doi:10.1016/j.pocean.2007.10.004.

Rippeth, T. P., M. R. Palmer, J. H. Simpson, N. R. Fisher, and J. Sharples (2005), Thermocline mixing in summer stratified continental shelf seas, *Geophys. Res. Lett.*, *32*, L05602, doi:10.1029/2004GL022104.

Rogashev, K. A., E. C. Carmack, and A. S. Salomatin (2000), Strong tidal mixing and ventilation of cold intermediate water at Kashevarov Bank, Sea of Okhotsk, *J. Oceanogr.*, *56*, 439–447.

Smith, G. C. (2005), The Gulf of St. Lawrence in winter: Tides, mixing and watermass transformation, Ph.D. thesis, McGill Univ., Montreal, Que., Canada.

Smith, G., F. Saucier, and D. Straub (2006a), Formation and circulation of the cold intermediate layer in the Gulf of Saint Lawrence, *J. Geophys. Res.*, *111*, C06011, doi:10.1029/2005JC003017.

Smith, G., F. Saucier, and D. Straub (2006b), Response of the lower St. Lawrence estuary to external forcing in winter, *J. Phys. Oceanogr.*, *36*, 1485–1501.

Stigebrandt, A. (1976), Vertical diffusion driven by internal waves in a sill fjord, *J. Phys. Oceanogr.*, *6*, 486–495.

Stigebrandt, A. (1979), Observational evidence for vertical diffusion driven by internal waves of tidal origin in the Oslofjord, *J. Phys. Oceanogr.*, *9*, 435–441.

Tamdrari, H., M. Castonguay, J.-C. Brêthes, P. Galbraith, and D. Duplisea (2011), The dispersal pattern and behaviour of cod in the northern Gulf of St. Lawrence: Results from tagging experiments, *Can. J. Fish. Aquat. Sci.*, in press.

Thorpe, S. A. (2007), *An Introduction to Ocean Turbulence*, 1st ed., 240 pp., Cambridge Univ. Press, New York.

Toole, J. M., R. W. Schmitt, and K. L. Polzin (1997), Near–boundary mixing above the flanks of a midlatitude seamount, *J. Geophys. Res.*, *102*(C1), 947–959.

Tuzhilkin, V. S. (2008), Thermohaline structure of the sea, in *The Black Sea Environment*, vol. 5, *The Handbook of Environmental Chemistry*, edited by A. G. Kostianoy and A. N. Kosarev, pp. 217–253, Springer, Berlin, doi:10.1007/6985_077.

D. Bourgault and F. Cyr, Institut des Sciences de la Mer de Rimouski, Université du Québec à Rimouski, 300 All. des Ursulines, CP 3300, succ. A, Rimouski, QC G5L 3A1, Canada. (frederic.cyr@uqar.qc.ca)

P. S. Galbraith, Ocean and Environmental Science Branch, Maurice-Lamontagne Institute, Fisheries and Oceans Canada, 850 Rte. de la Mer, CP 1000, Mont-Joli, QC G5H 3Z4, Canada.